POLITECNICO
MILANO 1863

SCUOLA DI INGEGNERIA INDUSTRIALE
E DELL'INFORMAZIONE

Executive Summary of the Thesis

Investigation of matrix effects on laser-induced plasmas

Laurea Magistrale in Nuclear Engineering - Ingegneria Nucleare

Author: Lorenzo Bonelli

Advisor: Prof. Christoph Gerhard

Academic year: 2025-2026

Abstract

This thesis investigates and characterizes matrix effects in Laser-Induced Breakdown Spectroscopy (LIBS), with particular focus on how crystal structure and material phase influence plasma properties. To this end, different structural forms of SiO_2 and Al_2O_3 were studied. For SiO_2, α-crystalline quartz and amorphous fused silica (Infrasil) were analyzed, while for Al_2O_3 the comparison involved α-crystalline sapphire and ceramic polycrystalline alumina. These materials were selected to isolate the role of structural order and phase composition in plasma formation and evolution. LIBS measurements were performed under controlled experimental conditions, and the acquired spectra were analyzed using the Calibration-Free LIBS (CF-LIBS) approach. By systematically varying the gate width and the delay time, the temporal evolution of the plasma temperature $T(t)$ and electron number density $n_e(t)$ was reconstructed. Comparing the plasma parameters obtained for the different material structures enabled assessing the time-dependent contribution of matrix effects and their correlation with crystallinity and material phase. This work contributes to a deeper understanding of the physical origin of matrix effects in LIBS and provides insights to improve the robustness of CF-LIBS quantitative analysis.

Keywords: LIBS; CF-LIBS; matrix effects; plasma diagnostics; laser–matter interaction; laser–plasma interaction; LTE.

Introduction

Laser-Induced Breakdown Spectroscopy (LIBS) is an atomic emission technique in which a pulsed laser produces a transient microplasma from the target surface; the emitted radiation provides the elemental "fingerprint" of the ablated material [3, 5]. Quantitative LIBS is complicated by *matrix effects*: the analytical signal depends not only on the elemental concentration, but also on how the material absorbs the laser energy, ablates, and forms an emitting/absorbing plume.
Calibration-Free LIBS (CF-LIBS) was introduced to reduce this dependence by coupling plasma diagnostics (temperature and electron density) with a physics-based emission model, avoiding external calibration curves [1, 2, 8].

1. Theoretical background

A LIBS measurement consists of (i) laser–matter interaction and ablation, (ii) plume/plasma formation and expansion, and (iii) optical emission detection. The spectrum typically evolves from an early continuum-

dominated stage (free–free and free–bound emission) to ionic lines and later to neutral lines; therefore, gated detection (delay time and gate width) is essential to select a meaningful plasma phase for diagnostics and quantification [7].

Under suitable conditions, the plasma can be treated with an equilibrium description (commonly LTE, possibly with multi-zone corrections). Then, line intensities can be related to level populations via the Boltzmann distribution, yielding the temperature through a Boltzmann plot:

$$\ln\left(\frac{I_{ul}\,\lambda}{A_{ul}\,g_u}\right) = -\frac{E_u}{k_B T} + \text{const.}$$

The electron density n_e is obtained from Stark broadening [9]

$$n_e = \frac{\Delta\lambda_{1/2}}{2\,w(T)}\,10^{16}\,\text{cm}^{-3}, \tag{1}$$

or from ionization balance (Saha/Saha–Boltzmann). A common LTE ionization relation is:

$$\frac{N_{II}}{N_I} \propto \frac{1}{n_e}\,T^{3/2}\,\exp\left(-\frac{E_{\text{ion}}}{k_B T}\right).$$

Finally, elemental fractions are inferred from the set of measured lines and closed by imposing $\sum_A C_A = 1$ [6]. In practice, the accuracy critically depends on line selection, spectroscopic data quality, stationarity within the gate, and optical thickness/self-absorption of the lines [10].

Matrix effects arise because the same incident laser pulse does not generate the same ablated mass, plasma density/volume, or energy-coupling history for different materials. Even at fixed stoichiometry, changes in (i) optical properties, (ii) thermophysical properties, and (iii) microstructure can modify ablation efficiency and plume conditions. These variations propagate differently into $T(t)$ and $n_e(t)$, and result into different degrees of self-absorption or plasma shielding, biasing both classical calibration and CF-LIBS [5, 10].

2. Experimental approach

All measurements were performed under controlled and repeatable conditions using a commercial enclosed LIBS platform equipped with a Q-switched Nd:YAG source at 1064 nm, gated detection, and a high-resolution spectrometer. To mitigate shot-to-shot variability and local surface heterogeneity, each condition is obtained by averaging multiple single-shot spectra acquired at different positions on the sample surface (order of $N \sim 100$).

The investigated materials were selected to isolate structural contributions at fixed nominal stoichiometry:

- SiO_2: α-quartz (crystalline) vs fused silica (Infrasil, amorphous);
- Al_2O_3: sapphire (α-Al_2O_3 single crystal) vs polycrystalline alumina ceramic.

The plasma evolution is probed by varying the detector delay t_{delay} and gate width t_{gate}. At each temporal setting, CF-LIBS diagnostics are applied to obtain T and n_e; repeating the procedure across delays reconstructs $T(t)$ and $n_e(t)$. The comparison of these curves across material pairs provides a direct, time-resolved indicator of matrix effects due to crystallinity/phase.

3. Experimental results

Obtaining spectra suitable for CF-LIBS requires a careful optimization of the acquisition parameters. For this reason, two preliminary studies were carried out: (i) a surface-cleaning analysis, aimed at minimizing contamination-driven lines, and (ii) an irradiation (fluence) study, aimed at maximizing the signal-to-noise ratio (SNR) while preserving the sample integrity.

3.1. Acquisition protocol and data handling

LIBS spectra can be strongly affected by surface contamination. A common mitigation strategy consists of performing a sequence of *cleaning shots* on the same position before acquiring the spectrum used for analysis, so as to reduce the contribution of surface-related elements. Throughout this work, two cleaning shots at $E_{\text{laser}} = 8$ mJ were applied at each position.

The irradiation conditions were optimized by varying pulse energy and number of pulses. Single-shot operation resulted in less stable plasma conditions; therefore, a multi-pulse strategy was adopted. In the following, to increase both SNR and plasma stability, the configuration $E_{\text{laser}} = 5$ mJ with 8 pulses is used

for the acquisition shots.
The final acquisition protocol is:

- two cleaning shots at $E_{\text{laser}} = 8$ mJ;
- eight acquisition pulses at $E_{\text{laser}} = 5$ mJ.

A critical step for repeatable and reliable CF-LIBS analysis is the selection of suitable reference lines. The reference transitions adopted are the Si I line at $\lambda = 390.5523$ nm and the Al II line at $\lambda = 281.6185$ nm; the selection was guided by line quality and stability and by previous studies on similar materials [4].
The detection system includes two spectrometers: one covering the UV range (190–430 nm) and the other the visible range (405–800 nm). Since the two channels cannot be acquired on exactly the same plasma event, UV and visible spectra were collected on two nearby positions under identical experimental settings and then merged into a single spectrum after response correction by matching the overlap region (405–430 nm). For each time point, three UV and three VIS spectra were acquired and merged into nine UV–VIS combinations. Since the merged spectra are not strictly independent, a conservative worst-case approach was adopted by treating the combinations as fully correlated when propagating uncertainties

$$\overline{X} = \frac{1}{n}\sum_{i=1}^{n} X_i, \qquad \sigma^2_{\overline{X}} = \frac{1}{n^2}\left(\sum_{i=1}^{n}\sigma_i\right)^2. \tag{2}$$

3.2. Temporal sampling and LTE screening

The temporal evolution $T(t)$ and $n_e(t)$ was reconstructed by varying delay time and gate width. The initial set of acquisition windows was chosen based on commonly used values in the literature [7] and then refined by inspecting the data dispersion. Only time points consistent with LTE were retained, based on the McWhirter criterion [5]

$$n_e \geq 1.6 \times 10^{12}\, T^{1/2} (\Delta E)^3, \tag{3}$$

and on the linearity of the Saha–Boltzmann plot.

3.3. Time-resolved plasma parameters and matrix-effect signature

In fig. 1 are reported the temporal evolution of $n_e(t)$ and $T(t)$ after LTE screening. For all investigated materials, $n_e(t)$ exhibits a clear monotonic decrease, consistent with plume expansion and electron-ion recombination. Within uncertainties, no systematic differences between crystalline and amorphous/polycrystalline structures emerge in $n_e(t)$. The main material-dependent signatures are instead observed in the temperature evolution.

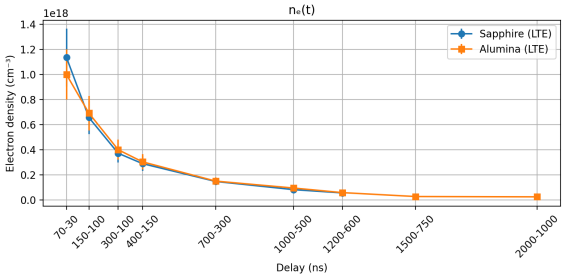

(a) $n_e(t)$ for Al_2O_3

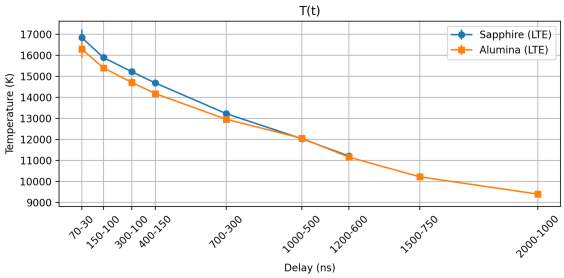

(b) $T(t)$ for Al_2O_3

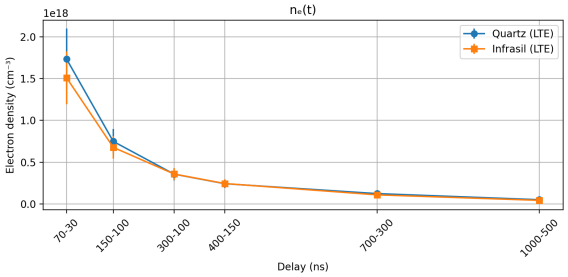

(c) $n_e(t)$ for SiO_2

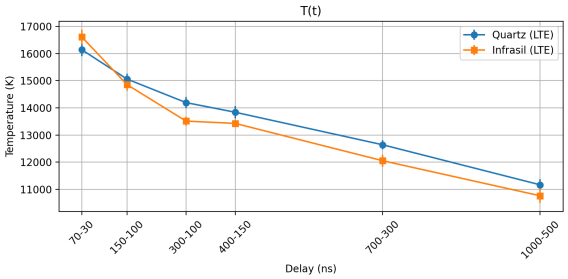

(d) $T(t)$ for SiO_2

Figure 1: Plasma-parameter evolution after LTE screening (McWhirter criterion and Saha–Boltzmann consistency).

To compactly compare decay rates, the post-screening trends were parameterized with exponential laws (fig. 2). For $T(t)$, two regimes are typically observed: an early-time faster decay, which is sensitive to the initial conditions set by laser–material coupling and ablation, and a later-time slower decrease, which is progressively governed by expansion and cooling in the surrounding gas. This transition is consistent with the progressive shift from ionic-rich emission to neutral-dominated emission, as qualitatively indicated by the increase of n_I/n_{II} (fig. 3).

SiO_2: quartz vs Infrasil. For SiO_2, Infrasil exhibits a higher initial plasma temperature than crystalline quartz. A consistent interpretation is that, at the laser wavelength used in this work, Infrasil is characterized by stronger effective absorption and lower thermal conductivity than quartz, promoting a more spatially confined energy deposition near the surface. This increases the effective energy per unit ablated mass and results in a steeper early-time temperature decay [11]. At later times, the temperature trends become more similar, consistent with an evolution increasingly governed by plume expansion and recombination rather than by the details of the initial coupling.

Al_2O_3: sapphire vs alumina. For Al_2O_3, the reconstructed temperature decays are broadly comparable and show only modest differences within uncertainties. This weaker contrast is consistent with smaller systematic differences in bulk thermophysical properties between sapphire and dense alumina, and with competing microstructure-driven effects in the ceramic (e.g. grain boundaries, scattering-driven coupling, residual porosity/roughness), which can partially mask systematic early-time trends.

3.4. Initial temperature analysis (qualitative)

In addition to the room-temperature dataset, an auxiliary test was performed by varying the *initial* sample temperature prior to acquisition. Specimens were cooled down to approximately $-10\,^{\circ}\mathrm{C}$ or heated up to approximately $50\,^{\circ}\mathrm{C}$ and then measured.
The full CF-LIBS workflow did not yield sta-

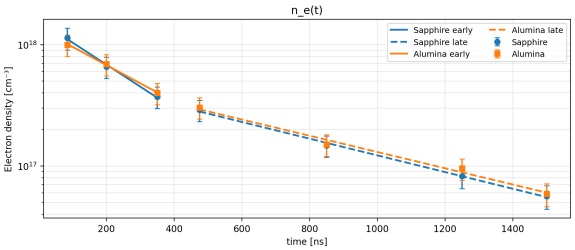

(a) $n_e(t)$ for Al_2O_3

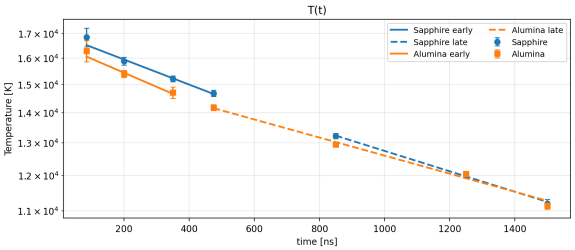

(b) $T(t)$ for Al_2O_3

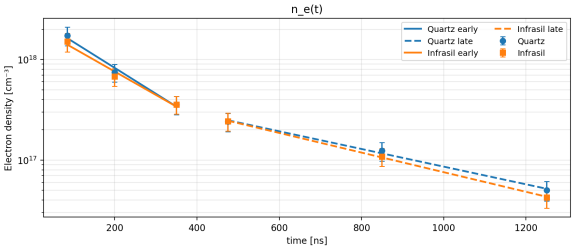

(c) $n_e(t)$ for SiO_2

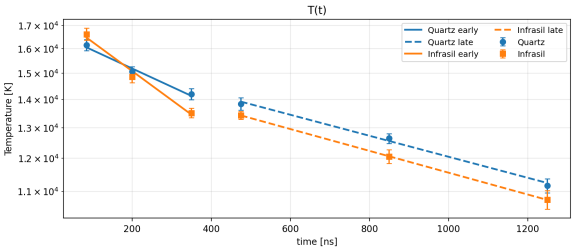

(d) $T(t)$ for SiO_2

Figure 2: Exponential fits of the plasma-parameter evolution after LTE screening. Fits are performed only on time points for which LTE is simultaneously satisfied by both samples in each material pair.

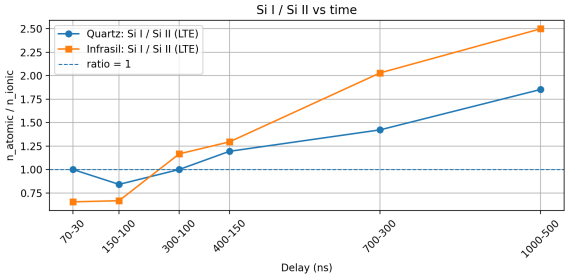

(a) SiO_2

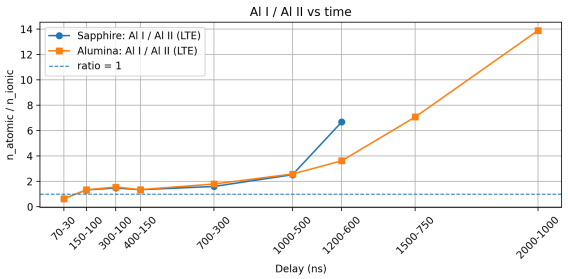

(b) Al_2O_3

Figure 3: Temporal evolution of the ratio between the number of identified neutral and singly-ionized lines (n_I/n_{II}). The increase of n_I/n_{II} indicates the progressive dominance of neutral emission due to recombination as the plasma cools and expands.

ble quantitative results for these datasets, because the sample temperature is not constant during acquisition and can drift while averaging over many positions, altering laser–material coupling and plasma formation conditions in a non-reproducible way. Therefore, the following discussion is restricted to qualitative spectral trends. In particular, the cold-start condition produces the dominant perturbation: a pronounced reduction of the overall emission is observed, plausibly linked to surface adsorption/condensation and to the resulting change in effective absorbed fluence. Representative peak heights are reported in tables 1 and 2.

Line	Sample	Ambient	Cooled	Heated
Si I	Infrasil	2578	220	2139
$\lambda = 390.5523$ nm	Quartz	1683	256	1556
Hα	Infrasil	311	631	212
$\lambda = 656.28$ nm	Quartz	276	208	235

Table 1: Peak heights (a.u., local baseline-subtracted) for selected features in the SiO_2 initial-temperature test.

Line	Sample	Ambient	Cooled	Heated
Al II	Sapphire	42545	867	50185
$\lambda = 281.6185$ nm	Alumina	43413	15176	46362
Hα	Sapphire	969	384	676
$\lambda = 656.28$ nm	Alumina	1048	908	1166

Table 2: Peak heights (a.u., local baseline-subtracted) for selected features in the Al_2O_3 initial-temperature test.

4. Conclusions and outlook

This thesis investigated and characterized matrix effects in Laser-Induced Breakdown Spectroscopy (LIBS) by comparing material pairs with identical empirical formula but different structural states: crystalline quartz versus amorphous fused silica (Infrasil) for SiO_2, and single-crystal sapphire versus polycrystalline alumina ceramic for Al_2O_3. The central methodological choice was to use time-resolved acquisition and a CF-LIBS workflow to reconstruct the temporal evolution of plasma temperature $T(t)$ and electron number density $n_e(t)$ under controlled instrumental conditions.

Main findings

- **Matrix effects are strongly time-dependent and are most visible at early delays.** At early times, the plasma state retains a strong memory of laser–material coupling and ablation efficiency, while at later times the evolution becomes progressively governed by plume expansion and cooling in the ambient gas, reducing material-dependent differences.
- **$n_e(t)$ is broadly similar across matrices, while $T(t)$ carries the clearest material signature.** Within uncertainties, no systematic separation emerges in $n_e(t)$, whereas $T(t)$ shows reproducible matrix-dependent trends.
- **SiO_2: quartz vs Infrasil.** Infrasil yields higher early-time temperatures and a steeper early-time decay, consistent with more spatially confined energy deposition and reduced heat diffusion into the bulk.
- **Al_2O_3: sapphire vs alumina.** Differences are weaker and partly masked by competing microstructure-driven effects in the ceramic, while late-time behavior converges for both samples.

Implications and outlook

A key implication is that matrix effects should not be treated as a single static correction, but rather as a time-dependent contribution that can be experimentally modulated. Later observation windows are generally advantageous for robustness because they reduce the impact of matrix-dependent initial conditions; however, excessively late gating can reduce ionic-line intensity and limit ion-based diagnostics, so an optimal compromise window must be selected.
Future developments include expanding the same-stoichiometry material set to disentangle optical and thermophysical drivers, and redesigning the initial-temperature protocol with tighter thermal control (temperature-controlled holder, in-situ temperature monitoring, and reduced averaging) to enable quantitative CF-LIBS inversion under well-defined thermal states.

References

[1] A Ciucci, Michela Corsi, Vincenzo Palleschi, S Rastelli, Antonio Salvetti, and Elisabetta Tognoni. New procedure for quantitative elemental analysis by laser-induced plasma spectroscopy. *Applied spectroscopy*, 53(8):960–964, 1999.

[2] Gabriele Cristoforetti, Alessandro De Giacomo, M Dell'Aglio, Stefano Legnaioli, Elisabetta Tognoni, Vincenzo Palleschi, and Nicolo Omenetto. Local thermodynamic equilibrium in laser-induced breakdown spectroscopy: beyond the mcwhirter criterion. *Spectrochimica Acta Part B: Atomic Spectroscopy*, 65(1):86–95, 2010.

[3] Gábor Galbács. A critical review of recent progress in analytical laser-induced breakdown spectroscopy. *Analytical and bioanalytical chemistry*, 407(25):7537–7562, 2015.

[4] Christoph Gerhard, Sid Ahmed Beldjilali, Robert Köhler, Jan Gluth, Andreas Tümmel, Djoudi Bouhafs, Anne-Patricia Alloncle, Frédéric Pelascini, and Jörg Hermann. Investigation of solar cell cover glass surfaces after long-term exposure to desert climate in southern algeria. *The European Physical Journal Plus*, 140(9):818, 2025.

[5] David W Hahn and Nicoló Omenetto. Laser-induced breakdown spectroscopy (libs), part i: review of basic diagnostics and plasma—particle interactions: still-challenging issues within the analytical plasma community. *Applied spectroscopy*, 64(12):335A–336A, 2010.

[6] Jörg Hermann*. Calibration-free laser-induced breakdown spectroscopy. *Laser Induced Breakdown Spectroscopy (LIBS) Concepts, Instrumentation, Data Analysis and Applications*, 1:89–121, 2023.

[7] Wenqi Lei. *Temporal and spatial characteristics of laser-induced plasma on organic materials and quantitative analysis of the contained inorganic elements*. PhD thesis, Université Claude Bernard-Lyon I; East China normal university (Shanghai), 2012.

[8] Francesco Poggialini, Beatrice Campanella, Bruno Cocciaro, Giulia Lorenzetti, Vincenzo Palleschi, and Stefano Legnaioli. Catching up on calibration-free libs. *Journal of Analytical Atomic Spectrometry*, 38(9):1751–1771, 2023.

[9] Ashwin P Rao, Mark Gragston, Anil K Patnaik, Paul S Hsu, and Michael B Shattan. Measurement of electron density and temperature from laser-induced nitrogen plasma at elevated pressure (1–6 bar). *Optics express*, 27(23):33779–33788, 2019.

[10] Fatemeh Rezaei, Gabriele Cristoforetti, Elisabetta Tognoni, Stefano Legnaioli, Vincenzo Palleschi, and Ali Safi. A review of the current analytical approaches for evaluating, compensating and exploiting self-absorption in laser induced breakdown spectroscopy. *Spectrochimica Acta Part B: Atomic Spectroscopy*, 169:105878, 2020.

[11] Xuan Song, Xianqian Wu, Lanhong Dai, and Minqiang Jiang. Comparative study of amorphous and crystalline zr-based alloys in response to nanosecond pulse laser ablation. *Acta Mechanica Sinica*, 38(2):221480, 2022.